REVIEW

Whispering-gallery mode microcavity quantum-dot lasers

N.V. Kryzhanovskaya, M.V. Maximov, A.E. Zhukov

Abstract. **This review examines axisymmetric-cavity quantum-dot microlasers whose emission spectrum is determined by whispering-gallery modes. We describe the possible designs, fabrication processes and basic characteristics of the microlasers and demonstrate the possibility of lasing at temperatures above 100 °C. The feasibility of creating multichannel optical sources based on a combination of a broadband quantum-dot laser and silicon microring modulators is discussed.**

1. Introduction

The limitations imposed on the information transfer rate and transmission range by heat generation in metallic conductors led to a transition to optical communications. The transition first occurred in long-haul communications, but in recent years intensive research effort has been concentrated on optical systems suitable for use at ever shorter distances, e.g. for data transfer between computer boards or even within a single board.

In assessing the suitability of an optical source for data transfer within a board, the most important point is that the source should be small, which stems from both the small space available and the requirement of low pump power, because it scales roughly linearly with the area of the device. An example of compact optical sources is vertical-microcavity surface-emitting lasers, which possess record-low threshold currents (a lasing threshold below 100 μA was demonstrated as early as 1998 [1]). Recent years have seen considerable progress in raising the data rate to above 20 Gbit s⁻¹ through

direct modulation [2]. In particular, oxide-confined 850-nm vertical-cavity surface-emitting lasers have demonstrated data rates in the range 40–44 Gbit s⁻¹ [3, 4]. In addition, such lasers offer a record-low energy-to-data ratio and switching energy: under 100 fJ bit⁻¹ and under 100 mW Gbit⁻¹ s, respectively [5].

However, vertical emission, an advantage when the laser output is to be coupled into optical fibre, requires additional engineering tricks to couple the optical signal into a planar waveguide [6–8]. Moreover, vertically emitting lasers with characteristics suitable for optical communication systems have rather complex designs. This is not a serious problem in the case of long- and medium-haul communications, but the complicated fabrication and high cost of laser sources limit their use in the commercial-scale production of ultrashort-haul optical systems.

More attractive for use in future on-chip optical communication systems are microcavity lasers in which the beam is parallel to the plane of the structure. Such lasers with a microring resonator (MRR) or microdisk resonator (MDR) have recently been studied most extensively. Like most vertically emitting lasers, the microring and microdisk lasers are axisymmetric, but the highest quality factor (Q) in them is offered by whispering-gallery modes (WGMs), which circulate around the resonator circumference. Since a wave in WGM resonators is reflected from the lateral surface of the structure at a small grazing angle, they possess high Q and offer the possibility of low-threshold lasing, even though their dimensions are much smaller than those typical of Fabry–Perot laser cavities. Moreover, ensuring a large separation between neighbouring resonance wavelengths, the small dimensions of the WGM resonators help to achieve single-frequency lasing.

The first semiconductor lasers of the type in question were optically pumped InGaAsP/InP microdisk lasers containing quantum wells with an emission wavelength near 1.55 μm [9, 10]. They were followed by quantum-well injection structures [11–13]. Advances in the field of stripe-geometry lasers having an active region based on self-organised quantum dots (QDs) led researchers to focus on WGM microlasers containing QD arrays [14–16].

One key requirement for microlasers is high thermal stability: the ability to operate without any thermal stabilisation systems at elevated temperatures, expected when an emitter is located in the immediate vicinity of transistor logic components. In this respect, QDs have considerable potential due to their discrete energy spectrum, the deep localisation of the active region relative to the waveguide (at least in QDs grown on GaAs substrates and operating in the 1.3-μm range [17]) and the use of new temperature sensitivity suppression

N.V. Kryzhanovskaya St. Petersburg Academic University (Nanotechnology Research and Education Centre), Russian Academy of Sciences, ul. Khlopina 8/3, 194021 St. Petersburg, Russia; e-mail: kryj@mail.ioffe.ru;
M.V. Maximov Ioffe Physical Technical Institute, Russian Academy of Sciences, Politekhnicheskaya ul. 2, 194021 St. Petersburg, Russia; St. Petersburg Academic University (Nanotechnology Research and Education Centre), Russian Academy of Sciences, ul. Khlopina 8/3, 194021 St. Petersburg, Russia; e-mail: maximov@beam.ioffe.ru;
A.E. Zhukov St. Petersburg Academic University (Nanotechnology Research and Education Centre), Russian Academy of Sciences, ul. Khlopina 8/3, 194021 St. Petersburg, Russia; Ioffe Physical Technical Institute, Russian Academy of Sciences, Politekhnicheskaya ul. 2, 194021 St. Petersburg, Russia; e-mail: zhukov@beam.ioffe.ru

methods through modulation acceptor doping [18–20]. Currently, 1.3-µm surface-emitting QD lasers rated for operation up to 150 °C are in mass production [21], and the highest temperature at which cw operation has been demonstrated is 220 °C [22].

One of the properties that make QDs attractive for use as active regions of microlasers is lateral carrier transport suppression [23, 24], whereas charge carriers in structures containing a two-dimensional (2D) quantum well can readily reach the wall of the microresonator and, if the surface recombination rate is high (like in the AlGaInAs/GaAs material system), the radiative recombination efficiency drops drastically. By contrast, in the case of QDs charge carriers are rapidly captured at the dots and cannot move laterally. The higher the carrier localisation energy in QDs, the shorter the diffusion length and, accordingly, the weaker the effect of surface recombination.

## 2. Self-organised quantum dots and related lasers

QD arrays are semiconductor heterostructures in which the limiting (zero-dimensional) case of size quantisation takes place. Thus, QD lasers are a development of light-emitting semiconductor devices with a low-dimensional active region, which originated as quantum-well lasers [25]. Interest in the technology of QD fabrication and the use of QDs in lasers was caused to a significant degree by theoretical predictions by Arakawa and Sakaki [26] that the lasing threshold of QD lasers should be temperature-independent.

The most important results so far have been obtained using QD array self-organisation during the epitaxy of a semiconductor material differing in lattice parameter from the substrate by several per cent. The driving force of the morphological transformation of an elastically strained 2D layer into a QD array (Fig. 1) is the possibility to reduce the total energy of the lattice-mismatched system through partial elastic stress relaxation near the vertices of three-dimensional islands [27].

Lasers based on InAs/GaAs QDs produced via self-organisation during growth were first made in the mid-1990s at the Ioffe Physical Technical Institute, Russian Academy of Sciences [28, 29]. The two most important achievements pertaining to the ability to tailor the properties of QDs and having a very direct relation to the possibility of using QDs in lasers are the development of a procedure for producing multiply stacked QDs [30, 31] and the discovery of a method for controlling the emission wavelength by modifying the matrix material [32, 33].

The maximum optical gain attainable in a single-layer QD structure is relatively low, about 6 cm^{-1} [34]. Clearly, this is insufficient for overcoming optical losses that are present in most semiconductor lasers for practical application. At the same time, in the case of sequential growth of several layers of QDs, which is enabled by using thin interlayers (spacers) of unstrained material, the saturated gain increases approximately in proportion to the number of rows and may reach about 50 cm^{-1} [22, 35, 36] (Fig. 2).

The simplest way of controlling the emission wavelength of self-organised QDs is by increasing the effective thickness of the QD material, because this increases the size of the forming islands. In particular, by varying the thickness of the InAs layer from 1.7 monolayers (which corresponds to the onset of island growth) to 3.5 monolayers (the onset of plastic
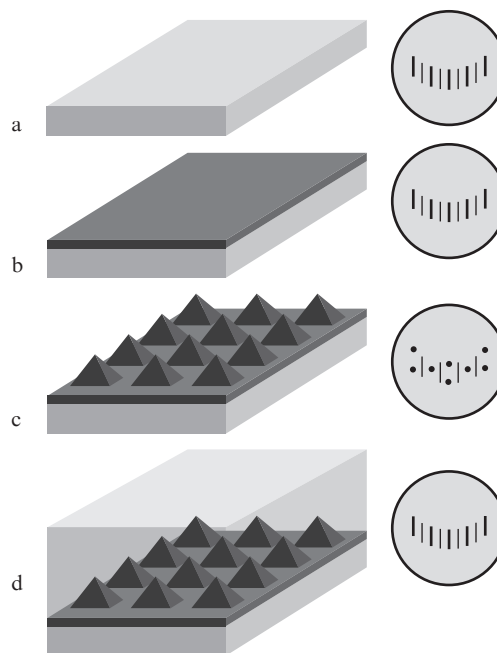

Figure 1. Schematic representation of InAs/GaAs QD fabrication steps (left) and corresponding high-energy electron diffraction patterns (right): (a) pristine GaAs surface, (b) deposition of InAs less than 1.7 monolayers in thickness, (c) growth of islands when the thickness of the InAs layer exceeds 1.7 monolayers, (d) capping of the InAs island array with a GaAs layer.
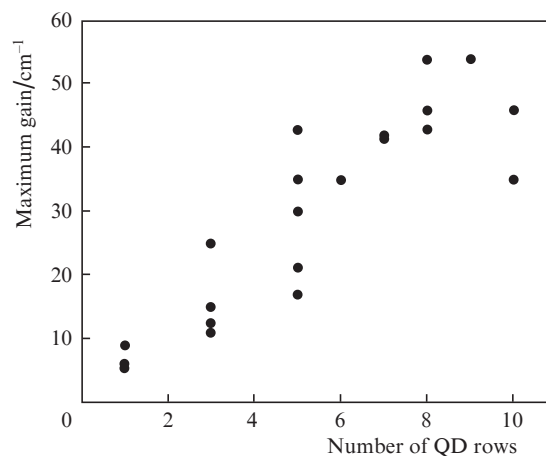
Figure 2. Relationship between the number of rows and the maximum (saturated) optical gain G_{sat} in QD lasers operating in the 1.3-µm range.

stress relaxation), the emission wavelength of QDs in a GaAs matrix can be tuned from 1.05 to 1.2 µm. This is, however, accompanied by changes in other characteristics of the QD array, including its surface density and size uniformity, which may have an adverse effect on the lasing performance. Moreover, deposition of too much InAs leads to dislocation generation.

Embedding a QD array in a narrower band gap matrix (e.g. in an InGaAs quantum well instead of a GaAs layer) increases the emission wavelength of the QDs [32, 33] (Fig. 3). This offers the possibility of precisely controlling the emission wavelength by varying the parameters (thickness and chemical composition) of the capping layer, whereas the other properties of the QD array remain essentially unchanged. At
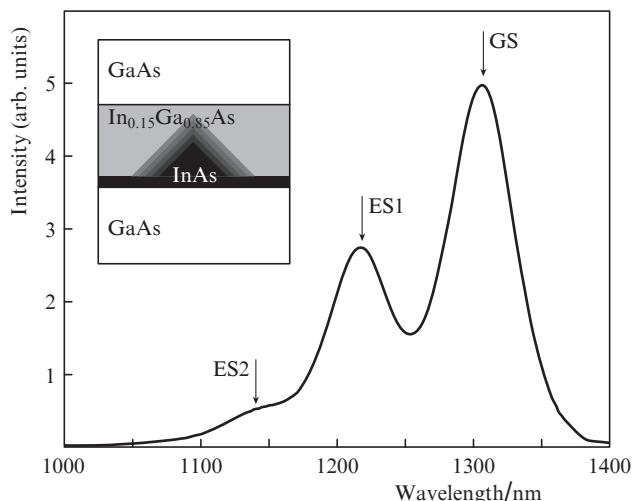
Figure 3. 300-K photoluminescence spectrum and schematic composition profile (inset) of InAs/InGaAs QDs. The arrows mark the ground (GS), first excited (ES1) and second excited (ES2) optical transitions of the QDs.

Figure 4. Echo Wall in the Temple of Heaven, Beijing, as an example of an acoustic WGM resonator: plan image and photograph (inset).

a particular combination of parameters, a wavelength above 1.3 μm can be reached, which opens up the possibility of using laser structures grown on GaAs substrates in optical communication systems.

Self-organised quantum dots, namely, InAs/InGaAs QDs with an emission wavelength near 1.3 μm, hold several records in the field of injection lasers, including the lowest threshold current density (under 10 A cm^{-2} [37, 38]), zero temperature sensitivity of power–current behaviour [20] and the possibility of high-speed data transmission without changes in modulation parameters in a wide temperature range [39].

3. Whispering-gallery mode resonators

It has become good form to begin the story about WGMs by mentioning the study of the acoustic properties of St Paul's Cathedral, London, by Lord Rayleigh. We will not skip this textbook example, and will add another World Heritage site that exhibits a similar acoustic effect: the Echo Wall in the Temple of Heaven in Beijing (Fig. 4). Describing the properties of the Whispering Gallery, Lord Rayleigh wrote: 'The whisper seems to creep round the gallery horizontally' [40]. A property common to these objects is that reflection of sound from walls results in the formation of a high-Q resonator for acoustic waves circulating around the wall.

Axisymmetric solid-state resonators are optical analogues of the above architectural objects. Even though optical WGMs were first observed in a resonator with a gain medium (samarium-doped fluorite [41]), researchers' interest was long concentrated on passive optical cavities, in which high and ultrahigh Q values can be achieved at small dimensions. In particular, Grudinin et al. [42] obtained Q near 6×10^{10} in a cylindrical CaF$_2$ resonator about 5 mm in diameter. The Q of microresonators in the form of silicon disks of 5 μm radius was $(5-10) \times 10^5$, and that of 30-μm-radius disks reached 5×10^6 [43, 44].

In what follows, we will be interested primarily in semiconductor MDRs or MRRs. These typically are relatively thin (a fraction of a micron) waveguide structures in the form of a disk or ring a few to tens of microns in diameter, surrounded by a lower refractive index material (e.g. by air).

The optical modes of a dielectric cylinder are characterised by three numbers (m, q and p for definiteness), which describe the spatial field distribution (the number of zeros) in the azimuthal direction, in radial direction and along the normal to the disk and determine the azimuthal, radial and vertical mode orders. The field is related to the azimuth angle φ by $\exp(\pm im\varphi)$, and the radial distribution within the cylinder is represented by mth-order cylindrical Bessel functions of the first kind, J_m.

At low m values and high q values, an optical mode is similar to a mode of the Fabry–Perot cavity (FPM) formed by the walls of the cylinder. At the same time, at high m and low q values the field distribution corresponds to a wave travelling in the peripheral part of the cylinder, i.e. to a whispering-gallery mode. The field distribution in these limiting cases
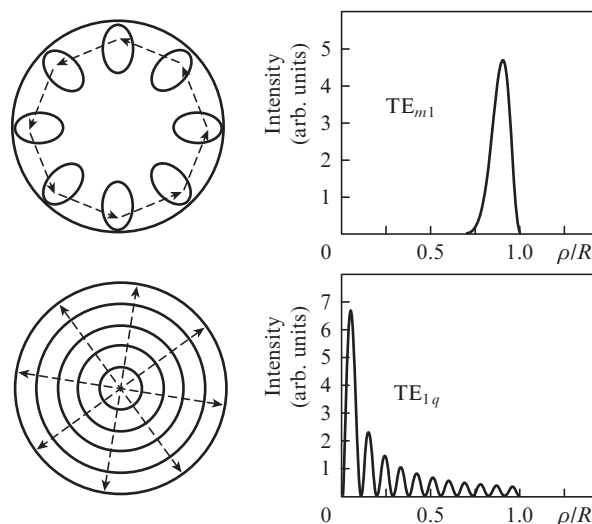
Figure 5. Schematic representation of the spatial field distribution of an optical mode (left) and the radial intensity distribution (right) for a WGM (top) and Fabry–Perot mode (bottom).

is schematically illustrated in Fig. 5. Figure 6 shows calculated spatial field distributions for different radial WGM orders. Also presented are emission intensity distributions obtained for a quantum-dot MRR by scanning an optical fibre over the microresonator surface (so-called near-field scanning optical microscopy), which allow one to visualise the spatial field distribution at a particular (resonance) wavelength.
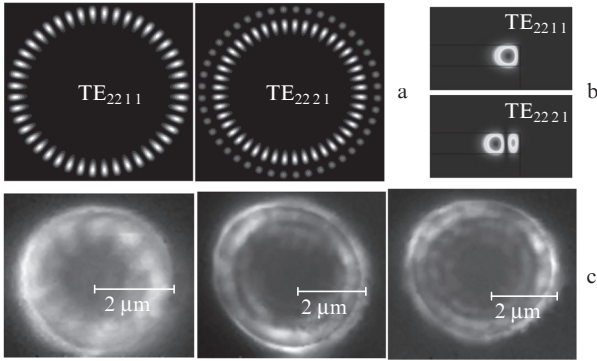
Figure 6. Calculated field distributions in a microdisk for WGMs of different orders: (a) top views, (b) side views; (c) near-field scanning optical microscopy images.

The Q-factor of FPMs is, as a rule, not very high (under 100), whereas WGMs typically have considerably higher Q (above 10^3). This is easy to understand given that WGMs are reflected at small grazing angles (in contrast to near normal incidence in the case of FPMs). Accordingly, WGMs show up in optical spectra as sharp peaks on top of the more gradual signal modulation due to FPMs. As an example, Fig. 7a shows emission spectra of an MDR and MRR containing a QD array. It is seen that the presence of a hole in the centre of a microdisk, i.e. a transition to a microring resonator, ensures Fabry–Perot mode suppression [45]. It also eliminates many lines due to high radial order WGMs.

The argument of the Bessel function representing the field distribution along the radial coordinate ρ is $(2\pi n/\lambda)\rho$, where n is the effective refractive index determined by the vertical waveguide structure and λ is the resonance wavelength. In a closed cylindrical resonator (e.g. in a dielectric cylinder coated with a metal), the allowed λ values can be found from boundary conditions. In the case of TM (TE) modes, i.e. modes with zero projection of the magnetic (electric) field onto the cylinder axis, the boundary condition is that the Bessel function (its derivative) should be zero on the lateral surface of the cylinder.

An open dielectric cylinder has hybrid optical modes, but they are treated as TM- or TE-like. As a rule, semiconductor microdisk lasers with an optical cavity sufficiently thin in the vertical direction have a single (fundamental) vertical mode and are dominated by TE-like modes. To a first approximation, the allowed wavelengths in a disk of radius R can be found from the condition that the field be zero on the disk surface [10]:

$$(2\pi n/\lambda)R = T_{mq}. \tag{1}$$

Here, T_{mq} is the qth root of the mth order Bessel function.

Relations that can be used to more accurately estimate the resonance wavelength and spatial mode distribution, in par-
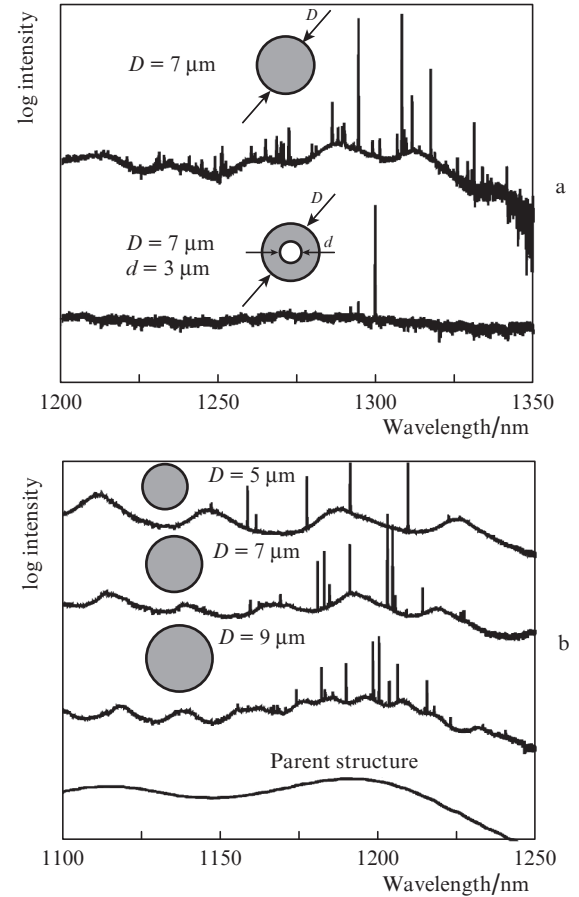
Figure 7. (a) 300-K photoluminescence spectra of an MDR and MRR having an outer diameter of 7 μm and containing an InAs/InGaAs QD array. (b) 78-K emission spectra of QD-containing MDRs of different diameters and spectrum of the parent epitaxial structure.

ticular for TM modes, with allowance for partial field penetration beyond the resonator are discussed in detail in Ref. [46]. In particular, field penetration beyond a resonator surrounded by air can be taken into account using a correction term, which should be subtracted from the right-hand side of (1): $(Pn\sqrt{n^2-1})^{-1}$. Here, $P = 1$ or $1/n^2$ for TE or TM modes, respectively.

Since at high m values and sufficiently low q values the roots of a Bessel function are approximately m (Fig. 8), it can be taken approximately in the case of large azimuthal WGM numbers that the resonance wavelength is independent of q and is given by

$$\lambda \approx 2\pi Rn/m, \tag{2}$$

which means that there are an integer number m of waves of wavelength λ/n along the circumference of a waveguide of length $2\pi R$.

Relation (2) can be used to derive a useful expression for the WGM free spectral range as a function of the circumference of the microresonator (note that the FPM free spectral range in a cylinder is determined by its diameter):

$$\text{FSR} \approx \frac{\lambda^2}{2\pi Rnf_{\text{gr}}}. \tag{3}$$

Here, the correction coefficient $f_{\text{gr}} = 1 + (\lambda/n)|\mathrm{d}n/\mathrm{d}\lambda|$ takes into account the variation of the refractive index with wavelength
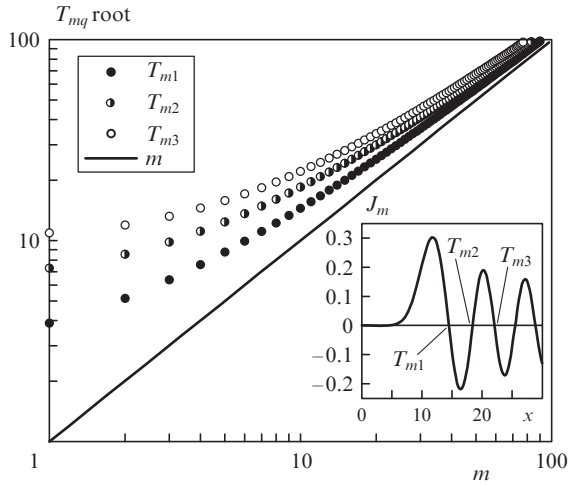
Figure 8. First three roots of the Bessel functions of the first kind, $J_m(T_{mq}) = 0$, against m and their approximate values. Inset: graph of $J_m(x)$ with $m = 10$.

[47]. It is typically near unity, but may reach 1.5 [10] when the wavelength approaches the absorption edge of one of the waveguide materials.

With decreasing R, the spectral separation between neighbouring resonances increases (Fig. 7b), reaching several tens of nanometres in micron-sized resonators. For example, at $n = 3$ the wavelength 1.3 μm in a 5-μm-radius GaAs-based resonator corresponds to an FSR of about 15 nm. In the case of vertical optical confinement due to air or an oxide layer, the effective refractive index may decrease, and the mode spacing may even increase.

The quality factor of a nonabsorbing resonator of an ideal shape, with axial symmetry, is determined by the radiation leakage loss. This so-called radiation quality factor, Q_{rad}, is an exponential function of the azimuthal number [9], so it increases rapidly with increasing resonator size (Fig. 9) and plays no significant role when the disk radius exceeds approximately 1 μm.

In practice, the Q-factor of a WGM resonator is determined to a significant degree by absorption. Note that the process dominating in passive silicon resonators is absorption in the near-surface region [43], whereas the determining process in III–V resonators (below threshold) is absorption in the active region [10]. Moreover, in the case of rough walls and small resonator dimensions, surface scattering may play a significant role.

In the case of QDs, the absorption in the active region, α_{act}, without pumping is approximately equal in magnitude to the maximum (saturated) gain G_{sat} in the QD array (Fig. 9, inset). The sum of the other optical losses (including the possible radiation leakage loss), α_{cav}, cannot exceed the saturated gain. Thus, the total loss in a cold resonator ($\alpha_{act} + \alpha_{cav}$) cannot exceed twice the saturated gain. Using the relation between the optical loss α in a resonator and its Q-factor,

$$Q \approx \frac{2\pi n}{\lambda \alpha}, \tag{4}$$

we can estimate the minimum value of G_{sat} necessary for lasing at varied Q of the resonator (Fig. 9). It is seen that $Q = 10^4$ corresponds to a saturated gain near 8 cm^{-1}. This is easily achievable even with one or two rows of QDs in the active region. At the same time, a transition to lasing in a microreso-
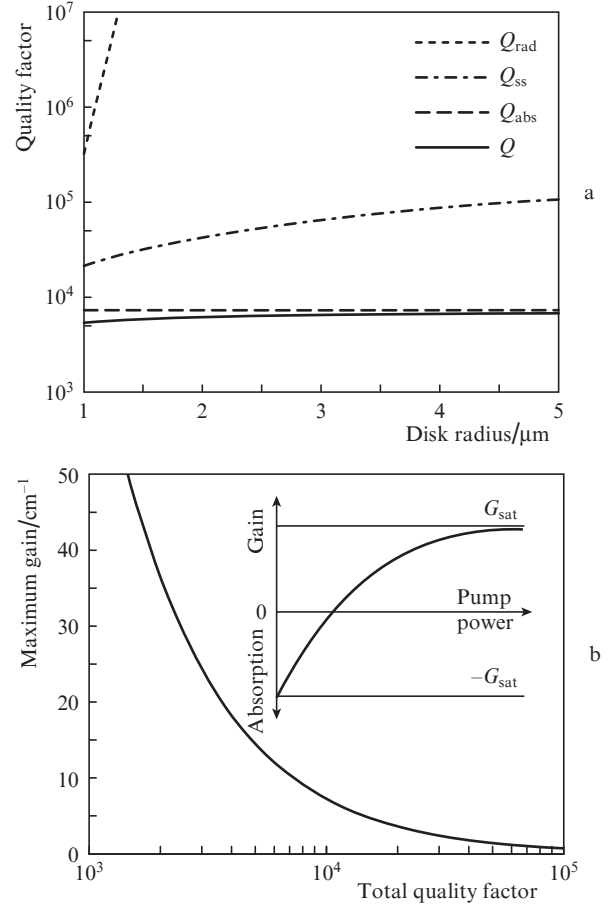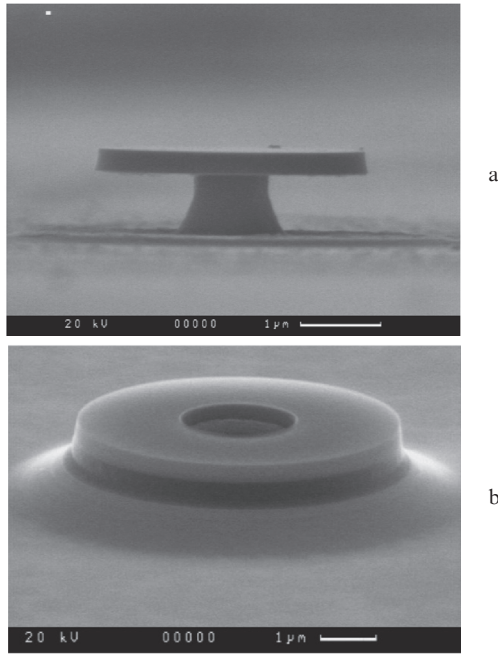

Figure 9. (a) Total quality factor Q and quality factors limited by emission (Q_{rad}), surface scattering (Q_{ss}) and absorption in QDs (Q_{abs}) as functions of MDR radius for the first radial mode (calculation for α_{act} = 20 cm^{-1}, a correlation length of 10 nm and an rms roughness height of 10 nm). (b) Relationship between the quality factor of a resonator and the optical gain in QDs necessary for lasing ($\lambda = 1.3$ μm, $n = 3$). Inset: schematic diagram of the optical absorption/gain in QDs against pump power.

nator with $Q = 10^3$ will require a QD array with a saturated gain above 50 cm^{-1}. These estimates highlight, on the one hand, that there are rather stringent requirements for the quality of the microresonator fabrication process and, on the other, that it is necessary to use multiply stacked QDs and ensure a high optical confinement factor of the active region in the waveguide of the WGM resonator.

4. Designs of WGM resonators based on III–V materials

The most widespread types of WGM microresonators based on III–V materials are a suspended disk resonator and a mesa structure in the form of a surface disk or surface ring. Figure 10 shows micrographs of these designs. It is also worth mentioning a less widespread type of WGM resonator: a micropillar.

In most designs, lateral optical confinement is provided by the semiconductor–air optical contrast, which ensures the maximum possible refractive index difference. The main distinctions between the designs are related primarily to the approaches used to ensure optical confinement in the vertical direction, because insufficient confinement may lead to an

accommodates a multilayer QD array. The thickness δ of the waveguide core, which supports only the fundamental mode, can be roughly estimated from the condition $\delta < \lambda/(2\sqrt{n_2^2 - n_1^2})$, where n_2 and n_1 are the refractive indices of the waveguide and cladding materials. In typical cases, δ does not exceed a fraction of a micron.

Figure 10. Scanning electron microscopy images of WGM resonators in the form of a (a) suspended disk and (b) microring mesa structure.

Figure 11. Principal processing steps in the fabrication of an MDR with an oxide underlayer: (a) epitaxial growth of a QD structure, (b) mesa structure production by reactive ion etching (RIE), (c) selective oxidation of the Al-containing underlayer.

increase in optical loss through optical mode leakage to the cladding layers. In particular, Kryzhanovskaya et al. [48] examined how parameters of an AlGaAs$-$(AlGa)$_x$O$_y$ pedestal layer influenced the performance of WGM QD lasers and showed that reducing the oxidation depth decreased the intensity of WGM lines, increased the lasing threshold and reduced the Q-factor because of an increased radiation leakage to the substrate region.

A distinctive feature of the suspended disk resonator is a relatively thin post connecting the disk proper to the substrate. Thus, the MDR material is confined by air in both the lateral and vertical directions (at least in the peripheral part of the disk). Because of this, the thickness of the disk is much smaller than its diameter. The post is produced by selective etching of a buffer layer consisting of aluminium-rich AlGaAs in GaAs-based structures and of indium phosphide in InGaAsP structures.

In the case of micropillars (see e.g. Ref. [49]), the height of the structure is several times its diameter. Vertical confinement is ensured by distributed Bragg reflectors. Because of their large thickness, deep etching is needed, so such structures are of little utility for coupling with planar waveguides. It is essentially impossible to produce MRRs in them.

In a circular mesa structure, optical confinement in the vertical direction is typically ensured by the semiconductor$-$air refractive index contrast on the top surface and by using a lower index semiconductor cladding or oxide layer at the bottom. As a result, the thickness of this structure is considerably smaller than its diameter, and both microdisk and microring resonators can be produced. Moreover, both optical and injection pumping is possible, and the output beam can be coupled into a nearby waveguide (e.g. a ridge waveguide [50]).

Figure 11 schematically illustrates one process for the fabrication of a QD microdisk resonator with a lower oxide cladding. The first step is the growth of an epitaxial structure containing an AlGaAs underlayer and GaAs optical core, which
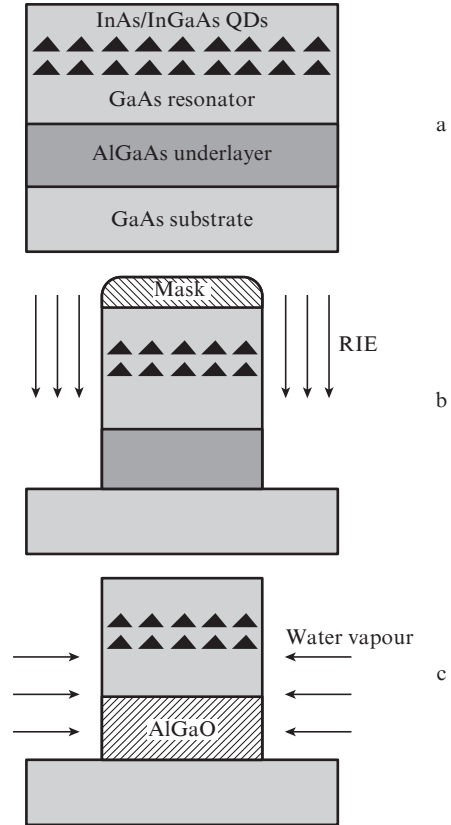
The mesa structure can be produced with the use of a mask by reactive ion etching or Ar$^+$ beam etching, as well as by using liquid etchants. As a rule, ion etching allows one to produce more vertical microresonator walls but causes surface damage, whereas wet etching causes less surface damage, but it may produce sloping walls. Moreover, the rate of such etching often depends significantly on the chemical composition of the semiconductor material, which may lead to lateral etching. In some instances, the last property can be used, e.g., to produce a narrow base of a suspended disk. In this context, it is worth mentioning recent work by Mao et al. [51], who took advantage of the considerably higher etching rate of Al$_{0.8}$Ga$_{0.2}$As in HF solution in comparison with GaAs in order to reduce the cladding radius relative to the waveguide radius. As a result, stronger optical confinement in the peripheral part of the disk helped to suppress leakage to the claddings for the lowest radial WGM orders.

At a very high percentage of aluminium in the Al$_x$Ga$_{1-x}$As underlayer ($x \approx 97\%$ to 99%), it can be converted to an Al$_x$Ga$_{1-x}$O$_y$ oxide by selective oxidation in water vapour at elevated temperatures [52]. The considerably lower refractive index of the oxide (about 1.7) in comparison with the unoxi-

dised semiconductor layer (above 3) ensures strong optical mode confinement in the vertical direction. At the same time, it should be taken into account that, even though the oxide ensures better heat removal from the active region than does air, its thermal conductivity is lower than that of the semiconductor layers.

## 5. MDR and MRR lasers with a QD active region

Even though the coupling of output radiation into a planar waveguide and injection pumping are difficult to achieve in suspended disk structures, it is this configuration that was used in both the first quantum-well microdisk laser (in 1992 [9]) and the QD structure in which WGMs were first observed (in 1999 [14]). Research interest in suspended disk structures is aroused by the possibility to obtain a low level of losses in such resonators owing to strong optical confinement. In a recent study [53], the optical quality of a QD-containing suspended MDR was assessed by transmission measurements in the 1.4-μm range, where the active region had no absorption. The measured resonance linewidth (4.1 pm) corresponds to a Q-factor of 3.6×10^5. Note that this high Q allows such QD microresonators to be employed in cavity quantum electrodynamics experiments [54].

The use of a suspended MDR enabled the first observation of lasing in a QD WGM resonator [15]. The active region used was a single InAs QD array in a GaAs matrix. The emission spectrum of an optically pumped 3-μm-diameter disk showed four sharp peaks in the spectral range 0.96–1 μm, which were identified as the $TE_{19\,1}$, $TE_{15\,2}$, $TE_{18\,1}$ and $TE_{14\,2}$ modes. The onset of lasing was evidenced by a characteristic break in the integrated emission intensity as a function of pump power. In later work, lasing was demonstrated in optically pumped suspended disk structures at room temperature [55], including cw operation [56]. Compared to previously studied lasers of this type, which contained one or two rows of QDs, the number of QD layers was increased to five, which ensured an increase in gain. The emission wavelength of the QDs was near 1.3 μm (at 300 K), which ensured deeper carrier localisation, suppressing thermal carrier escape from the active region at elevated temperatures.

In a previous study [57], lasing under continuous optical pumping was demonstrated in an MDR that had the form of a mesa structure and also contained five rows of QDs emitting in the 1.3-μm range. It is of interest to note that the only variation from the preceding study by the same authors [58], where lasing had been demonstrated for the first time in a QD WGM resonator at room temperature, was that no suspended disk configuration was used. The AlGaO underlayer, which had previously served to support the microdisk, was not decreased in diameter, which allowed the thermal resistance of the structure to be reduced.

A similar structure having an MRR geometry with an outer diameter of 6 μm and inner diameter of 2 μm enabled a record-high lasing temperature of 107 °C among WGM cavity QD microlasers to be achieved [59] (Fig. 12). It is seen that MRR lasers have a small temperature coefficient of their emission wavelength, less than 0.1 nm K^{-1}, which is well below the variation of the emission wavelength with band gap in Fabry–Perot cavity QD lasers (about 0.5 nm K^{-1}). Like in the case of vertical-microcavity surface-emitting lasers, the reason for this effect in the MRRs is that, in both instances, the emission wavelength is determined not by the spectral position of the gain peak of the active region but by the resonator mode frequency (provided it lies within the gain spectrum). A temperature change ΔT leads to a refractive index change $\beta n \Delta T$ and a redshift of the resonance wavelength λ by $\Delta_T \approx \beta \lambda \Delta T$. With a temperature coefficient of the refractive index $\beta = 7 \times 10^{-5}$ K^{-1} at $\lambda \sim 1.3$ μm and $T = 300$ K [60], the shift Δ_T can be estimated at about 0.09 nm K^{-1}.
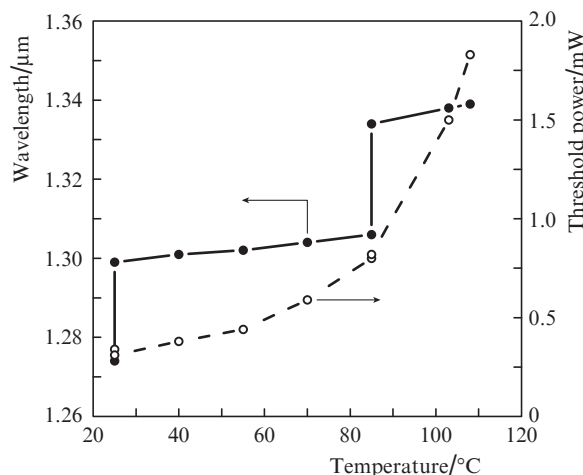

Figure 12. Temperature dependences of the emission wavelength and lasing threshold for a 7-μm-diameter MDR containing a QD array.

There is special practical interest in achieving single-frequency lasing, which can be ensured by reducing the microlaser dimensions. To our knowledge, the smallest cavity diameter at which room-temperature lasing has been achieved is 2.7 μm [61], whereas most of the MDRs and MRRs operating at room temperature have a size in the range 4.5 to 7 μm [51, 53, 55–57, 62]. Limitations on the minimum resonator size are associated with the fact that the lasing threshold increases with both decreasing resonator Q and increasing relative surface recombination contribution.

Even though, as mentioned above, the mode spacing in circular resonators several microns in diameter may exceed 20 nm, WGMs of various radial orders, if there are any, form their own sequences of resonances, which may overlap, thereby considerably complicating the optical spectrum. Since increasing the radial mode number q shifts the intensity maximum closer to the resonator axis, high radial WGM orders should be suppressed more strongly in a microring than in a microdisk of the same diameter. However, even in a microring laser with an inner diameter $d = 2$ μm and outer diameter $D = 6$ μm, the dominant modes are those with $q = 2$ and 3 [63]. Further increasing the inner diameter leads to a gradual decrease in lasing threshold, followed by a sharp increase starting at $d \approx 0.8D$ [61].

The complex mode structure of WGM resonators shows up as a large number of emission peaks in below-threshold spectra or in spectra obtained just above the lasing threshold (Fig. 13). However, as the pump power is raised further, the main line, whose position is the closest to that of the gain peak, begins to prevail. For QD MRRs, a side mode suppression ratio of 20 dB has recently been reported [45], suggesting quasi-single-mode lasing. The MRR whose laser emission spectra are presented in Fig. 13 is also of interest because it has been mounted on a silicon substrate [64]. The observed low-threshold lasing in such a structure leads us to conclude
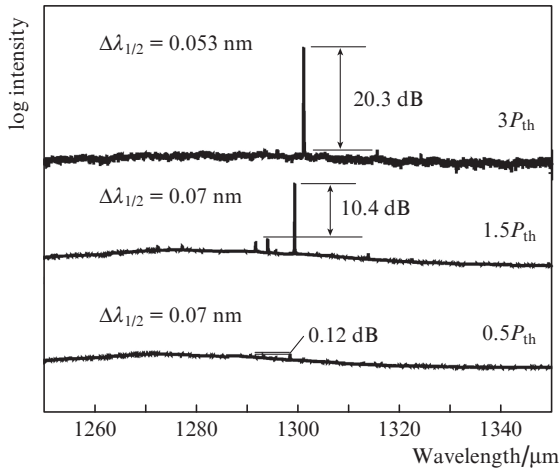
Figure 13. Room-temperature emission spectra of a QD MRR on silicon at different excitation powers (above and below lasing threshold P_{th}). $\Delta\lambda_{1/2}$ is the full width at half maximum.

that the hybrid integration of QD microlasers and silicon electronics is conceptually feasible.

To our knowledge, lasing in a QD MDR under injection pumping was first demonstrated in 2003 by Zhang and Hu [65]. They reported lasing at a temperature of 5 K in a suspended disk structure, with a top electrical contact made using an air bridge from Ti/Pt/Au between the top surface of the MDR and a contact pad produced on a Si_3N_4 insulating base.

Subsequently, injection lasers based on microdisk mesa structures were demonstrated, whose geometry was better suited to electrical pumping. Such structures can readily be planarised using an insulator with a window for the top electrical contact. One possible insulating coating material is benzocyclobutene [66], which combines the advantages of a low refractive index (near 1.5) and sufficiently high thermal conductivity (0.7 W m^{-1} K^{-1}). Using such a configuration, Mao et al. [51] achieved room-temperature lasing with a threshold of 0.45 mA in a 6.5-µm-diameter disk. In a simpler geometry of an 80-µm-diameter MRR, whose top surface was entirely covered with a metallic contact, cw lasing was demonstrated at temperatures of up to 50 °C [67]. It was also shown that increasing the inner diameter reduced the lasing threshold and suppressed high radial order modes.

Compared to suspended disk WGM resonators, planar MDRs and MRRs are easier to couple to various integrated optical devices. The output radiation of a microresonator can be coupled evanescently into a ridge waveguide located sufficiently closely to the microlaser in the same plane. Such radiation outcoupling from a ring laser having a QD active region but a millimetre-size resonator was reported by Cao et al. [68]. Another example of the possible integration of a WGM cavity laser and silicon photonics was described by Van Campenhout et al. [69]. An MDR of 7.5-µm diameter was produced from an InP-based epitaxial structure and then transferred to a silicon substrate containing a buried SiO_2 layer. The laser output was coupled into a silicon waveguide passing under the peripheral part of the MDR. The optical power coupled into the waveguide in continuous mode reached 10 µW at an efficiency of 20 µW mA^{-1}. Liang et al. [70] described a similar integration scheme, with the difference that the InP-based MRR laser was placed on a silicon

microdisk of the same diameter, and a ridge waveguide, also based on silicon, was produced in the plane of the microdisk. The structure was located over a buried oxide layer. Such integration schemes can be used as well in the case of QD microlasers.

6. Microring modulators

In contrast to WGM resonators containing an active region based on III–V materials, silicon-based resonators cannot emit light. At the same time, such 'passive' resonators allow one to control radiation emitted by another source and are thus of special interest. A planar structure composed of a passive MDR and two waveguides located on one substrate was first proposed by Marcatili [71] for realising an optical coupler filter (Fig. 14), in which, of many wavelengths propagating through one waveguide, only radiation corresponding to the resonance wavelength of the MDR would be transmitted to another waveguide. In this review, we will address the possibility of coupling such WGM resonators to broadband QD laser sources.
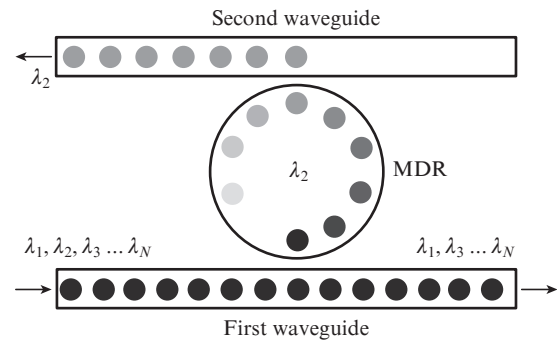
**Figure 14.** Schematic of an MDR-based integrated optical coupler filter.

A unique property of self-organised QDs, which finds a great diversity of applications, is that using them one can obtain very broad optical gain and laser emission spectra, which can reach 200 [72] and 75 nm [73, 74], respectively. The large width of the spectra is caused by the inhomogeneous broadening of the optical transitions of the QDs due to the scatter in island size, with further, deliberate broadening due to the use of several layers of QDs differing in centre wavelength and to the partial overlap of the ground and excited state optical transitions of the QDs.

Broad laser emission spectra are favourable for reducing the pulse duration in mode-locked lasers [75]. However, the key potential applications of lasers with broad emission spectra are in multichannel optical communication systems. The low relative intensity noise values (no worse than −125 dB Hz^{-1}) achievable in a selected mode of a Fabry–Perot laser cavity open up the possibility of using longitudinal modes as individual optical channels which can be modulated at a high rate (10 Gbit s^{-1} [76]).

A silicon MRR can be used as a wavelength-selective modulator of the QD laser output. The operating principle of such a compact, high-speed optical modulator [77] is illustrated in Fig. 15. The straight waveguide and ring microresonator are sufficiently close to each other for the laser radiation propagating through the waveguide to be coupled into

the microring, thereby reducing the output signal. The wavelength at which the transmission has a minimum corresponds to the resonance WGM of the microring resonator. Applying a voltage to the microring structure and thus changing the refractive index in it [78], one can tune the resonance wavelength λ_{res}, thereby controlling the transmission at the wavelength of some optical channel.
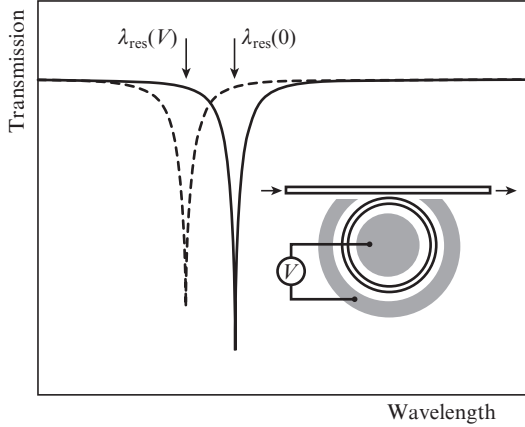

Figure 15. Schematic layout of a silicon MRR-based modulator and its transmission spectra at different voltages applied to the modulator.

Great potential for use in optical interconnects is offered by a combination of a broadband QD laser and a cascade modulator based on microring resonators tuned to different wavelengths. Compared to a multichannel optical system [79] consisting of several hybrid microring lasers based on III–V and silicon, whose radiation is coupled into one planar waveguide, the system based on a multiple-frequency QD laser is considerably easier to fabricate. In this case, one optical source ensures a spectral band several tens of nanometres in width. A version of such a system described by Gubenko et al. [80] is shown schematically in Fig. 16. The high uniformity of the QD laser output power spectral density [73] ensures that the individual channels have roughly equal powers, and the high stability of the QD laser output intensity after the separation into individual channels enables high-speed modulation of the channels.

Using a silicon p–i–n structure to produce silicon ring resonators of different radii in the range 4.98–5.04 μm, Xu et al. [81] have demonstrated the possibility of independent modulation of the output of a tunable laser at four distinct wavelengths near 1.55 μm at a rate of 4 Gbit s^{-1}. Later, the modulation rate in such structures was raised to 10–18 Gbit s^{-1} [82–84]. The possibility of modulating the intensity of one longitudinal mode of a multiple frequency QD laser by coupling its radiation into a 3-μm-diameter ring microresonator based on a silicon-on-insulator waveguide structure has been demonstrated by Wojcik et al. [85].

The resonance wavelength of a particular modulator in a cascade can be tuned by properly adjusting its size. The maximum size of a ring resonator, R_{max}, can be estimated using (3) from the condition that the spectral band Ω used for optical communications contains no more than one resonance frequency of the microring (Fig. 17):

$$R_{max} = \lambda^2/(2\pi n\Omega).\qquad(5)$$
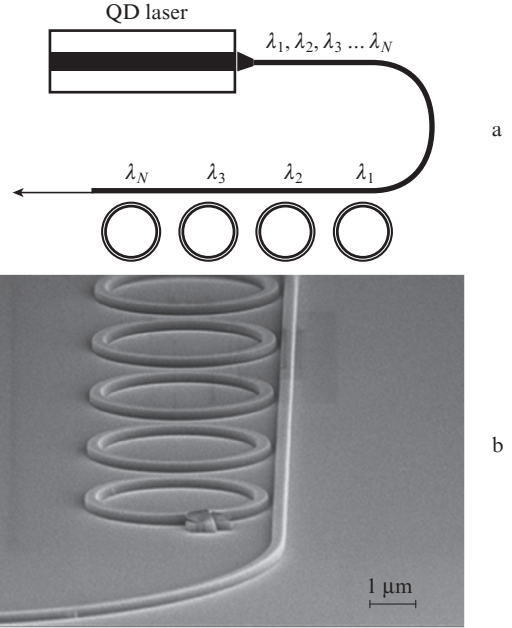
Figure 16. (a) Schematic of a multichannel optical source based on a broadband QD laser and MRR modulator cascade; (b) micrograph of a cascade modulator (courtesy of Innolume GmbH).
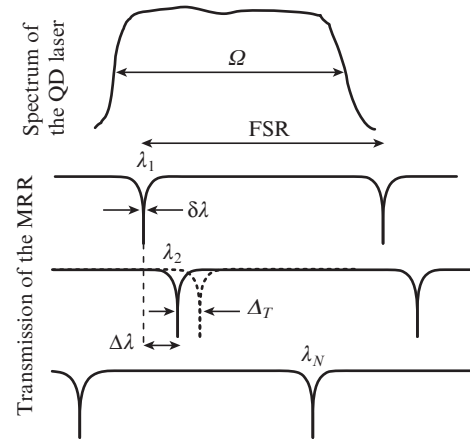
Figure 17. Relationship between spectral emission characteristics of a QD laser and MRR-based cascade modulator necessary for realising a multichannel optical source.

In our case, Ω is the width of the QD laser emission spectrum with a centre wavelength λ.

Changing the ring radius by ΔR changes the resonance wavelength by $\Delta\lambda \approx (\Delta R/R_{max})\lambda$. The number of channels, N, that can be accommodated within the emission spectrum of the QD laser is $(\Omega/\Delta\lambda) + 1$. Taking into account (5), we find that the maximum number of channels is

$$N_{max} = \lambda/(2\pi n\Delta R) + 1.\qquad(6)$$

Thus, when the resonance frequency is only controlled by varying the MRR size, the maximum number of channels is limited by the accuracy that can be warranted in producing MRRs of different diameters. Taking $\Delta R = 0.01$ μm (which seems to be the limit for reproducible technology at the pres-

ent stage), we find that N_{max} is just near eight at wavelengths around 1.3 µm.

To produce widely spaced resonance frequencies at nominally identical microresonator sizes and compensate for the unintended wavelength change caused by fabrication errors, one can use local heating [86–88], e.g. by an integrated heater. The temperature-induced change in optical path length in a semiconductor material is determined primarily by the temperature dependence of its refractive index. With the temperature coefficient of silicon $\beta \sim 5\times10^{-5}$ K^{-1} [60], we obtain a shift $\Delta_T \sim 0.07$ nm K^{-1}.

The change in resonance wavelength should exceed $\delta\lambda$ – the broadening of the line caused by the finite Q of the resonator and its splitting into a doublet because of the surface roughness, which lifts the degeneracy of clockwise- and counterclockwise-propagating modes [89, 90]. Even though Borselli et al. [44] reported silicon MDRs with a quality factor $Q > 10^6$ and relative splitting $Q_\beta \sim 3\times10^5$, silicon MRRs have lower optical performance ($Q = 2\times10^4$ and $Q_\beta \sim 3\times10^4$; see e.g. Ref. [81]), so a good estimate is $\delta\lambda \sim 0.1$ nm. Thus, the temperature of MRRs of the same size should be changed in at least 1.5 °C steps. Consequently, it appears quite reasonable to realise at least five to ten different resonance frequencies for a fixed resonator size. Given that this way of controlling the wavelength can be applied independently to MRRs of each size, the total number of channels will be about 50, which can be thought of as an on-chip optical system with wavelength-division multiplexing. Even if the modulation rate of one such channel is 10 Gbit s^{-1}, the total transfer rate of a QD laser-based multichannel source may reach 0.5 Tbit s^{-1}.

Note that there are also other possibilities to control the resonance wavelength. For example, Ikeda and Hane [91] reported a shift of a wavelength near 1.5 µm by 10 nm through an electromechanical displacement of a mobile part of a microresonator by 1 µm (which corresponded to a change in MRR size by 1.7 %). Among more exotic approaches, mention should be given to the possibility of tuning the wavelength by at least 0.5 nm via voltage-controlled coating of part of the waveguide of a polymer MRR with a droplet of liquid (aqueous Na_2SO_4 solution), which changes the effective refractive index [92].

7. Conclusions

Today, self-organised QDs are finding a new area of device applications, related to the possibility of using light-emitting devices with a QD active region for producing on-chip optical interconnects. The area of research that has been actively developed in recent years focuses on creating temperature-stable microdisk or microring lasers that can then be integrated with silicon photonics. In this area, lasing temperatures above 100 °C have been reached; the possibility to transfer microresonators to silicon without degradation of their performance has been demonstrated; cw lasing has been achieved, in particular under injection pumping; strong side mode suppression has been obtained; and low temperature sensitivity of the emission wavelength has been demonstrated.

These achievements are due to specific features of QD arrays, such as deep carrier localisation in the active region, the ability to tune their emission wavelength in a wide range (up to 1.3 µm) on GaAs substrates, suppression of sensitivity to recombination of the sidewalls, and the possibility of reaching high optical gain values through vertical multiplication of rows of QDs.

An alternative approach is being developed in parallel, which builds on a combination of a QD laser with a conventional resonator design, capable of lasing in a wide spectral range, and an array of modulators based on microring resonators. Only the first steps have been made to date in this direction, but it is expected to open up the possibility of realising on-chip optical systems with wavelength-division multiplexing.

References

1. Langenfelder T., Grothe H. *Electron. Lett.*, **34**, 2034 (1998).
2. Suzuki N., Hatakeyama H., Fukatsu K., Anan T., Yashiki K., Tsuji M. *Conf. OFC* (Anaheim, CA, USA, 2006) OFA4.
3. Blokhin S.A., Lott J.A., Mutig A., Fiol G., Ledentsov N.N., Maximov M.V., Nadtochiy A.M., Shchukin V.A., Bimberg D. *Electron. Lett.*, **45**, 501 (2009).
4. Westbergh P., Safaisini R., Haglund E., Kögel B., Gustavsson J.S., Larsson A., Geen M., Lawrence R., Joel A. *Electron. Lett.*, **48**, 1145 (2012).
5. Moser P., Hofmann W., Wolf P., Lott J.A., Larisch G., Payusov A., Ledentsov N.N., Bimberg D. *Appl. Phys. Lett.*, **98**, 231106 (2011).
6. Kash J.A., Doany F.E., Schares L., et al. *Conf. OFC* (Anaheim, CA, USA, 2006) OFA3.
7. Cheng J., Yang K., Patel K.M., Eustis T., Jin X.-J., Luong S.Q., Guilfoyle P.S. *Avionics, Fiber-Optics and Photonics Technol. Conf.* (Victoria, BC, Canada, 2007) p. 36.
8. Bardinal V., Camps T., Reig B., Barat D., Daran E., Doucet J.B. *Adv. Opt. Technol.*, **2011**, 609643 (2011).
9. McCall S.L., Levi A.F.J., Slusher R.E., Pearton S.J., Logan R.A. *Appl. Phys. Lett.*, **60**, 289 (1992).
10. Slusher R.E., Levi A.F.J., Mohideen U., McCall S.L., Pearton S.J., Logan R.A. *Appl. Phys. Lett.*, **63**, 1310 (1993).
11. Levi A.F.J., Slusher R.E., McCall S.L., Tanbun-Ek T., Coblentz D.L., Pearton S.J. *Electron. Lett.*, **28**, 1010 (1992).
12. Baba T., Fujita M., Sakai A., Kihara M., Watanabe R. *IEEE Photonics Technol. Lett.*, **9**, 878 (1997).
13. Fujita M., Inoshita K., Baba T. *Electron. Lett.*, **34**, 278 (1998).
14. Gayral B., Gerard J.M., Lemaitre A., Dupuis C., Manin L., Pelouard J.L. *Appl. Phys. Lett.*, **75**, 1908 (1999).
15. Cao H., Xu J.Y., Xiang W.H., Ma Y., Chang S.-H., Ho S.T., Solomon G.S. *Appl. Phys. Lett.*, **76**, 3519 (2000).
16. Michler P., Kiraz A., Zhang L., Becher C., Hu E., Imamoglu A. *Appl. Phys. Lett.*, **77**, 184 (2000).
17. Zhukov A.E., Kovsh A.R., Mikhrin S.S., Vasil'ev A.P., Semenova E.S., Maleev N.A., Ustinov V.M., Kulagina M.M., Nikitina E.V., Soshnikov I.P., Shernyakov Yu.M., Livshits D.A., Kryjanovskaya N.V., Sizov D.S., Maximov M.V., Tsatsul'nikov A.F., Ledentsov N.N., Bimberg D., Alferov Zh.I. *Phys. E*, **17**, 589 (2003).
18. Shchekin O.B., Deppe D.G. *Appl. Phys. Lett.*, **80**, 2758 (2002).
19. Fathpour S., Mi Z., Bhattacharya P., Kovsh A.R., Mikhrin S.S., Krestnikov I.L., Kozhukhov A.V., Ledentsov N.N. *Appl. Phys. Lett.*, **85**, 5164 (2004).
20. Tanaka Y., Ishida M., Takada K., Yamamoto T., Song H.-Z., Nakata Y., Yamaguchi M., Nishi K., Sugawara M., Arakawa Y. *Conf. CLEO* (San Jose, CA, USA, 2010) CTuZ1.
21. http://www.qdlaser.com.

22. Kageyama T., Nishi K., Yamaguchi M., Mochida R., Maeda Y., Takemasa K., Tanaka Y., Yamamoto T., Sugawara M., Arakawa Y. *Conf. CLEO* (Munich, Germany, 2011) PDA1.

23. Ouyang D., Ledentsov N.N., Bimberg D., Kovsh A.R., Zhukov A.E., Mikhrin S.S., Ustinov V.M. *Semicond. Sci. Technol.*, **18**, L53 (2003).

24. Moore S.A., O'Faolain L., Cataluna M.A., Flynn M.B., Kotlyar M.V., Krauss T.F. *IEEE Photonics Technol. Lett.*, **18**, 1861 (2006).

25. Dingle R., Henry C.H. U.S. Patent 3, 982, 207 (1976).

26. Arakawa Y., Sakaki H. *Appl. Phys. Lett.*, **40**, 939 (1982).

27. Shchukin V.A., Ledentsov N.N., Bimberg D. *Epitaxy of Nanostructures* (Berlin, Heidelberg: Springer-Verlag, 2004).

28. Ledentsov N.N., Ustinov V.M., Egorov A.Yu., Zhukov A.E., Maksimov M.V., Tabatadze I.G., Kop'ev P.S. *Fiz. Tekh. Poluprovodn.*, **28**, 1483 (1994).

29. Egorov A.Yu., Zhukov A.E., Kop'ev P.S., Ledentsov N.N., Maksimov M.V., Ustinov V.M. *8th Int. Conf. MBE* (Osaka, Japan, 1994) p.385.

30. Egorov A.Yu., Zhukov A.E., Kop'ev P.S., Ledentsov N.N., Maksimov M.V., Ustinov V.M., Tsatsul'nikov A.F., Bert N.A., Kosogov A.O., Bimberg D., Alferov Zh.I. *Fiz. Tekh. Poluprovodn.*, **30**, 1682 (1996).

31. Ustinov V.M., Egorov A.Yu., Kovsh A.R., Zhukov A.E., Maksimov M.V., Tsatsul'nikov A.F., Gordeev N.Yu., Zaitsev S.V., Shernyakov Yu.M., Bert N.A., Kop'ev P.S., Alferov Zh.I., Ledentsov N.N., Bohrer J., Bimberg D., Kosogov A.O., Werner P., Gosele U. *J. Cryst. Growth*, **175/176**, 689 (1997).

32. Zhukov A.E., Kovsh A.R., Egorov A.Yu., Maleev N.A., Ustinov V.M., Volovik B.V., Maksimov M.V., Tsatsul'nikov A.F., Ledentsov N.N., Shernyakov Yu.M., Lunev A.V., Musikhin Yu.G., Bert N.A., Kop'ev P.S., Alferov Zh.I. *Fiz. Tekh. Poluprovodn.*, **33**, 180 (1999).

33. Ustinov V.M., Maleev N.A., Zhukov A.E., Kovsh A.R., Egorov A.Yu., Lunev A.V., Volovik B.V., Krestnikov I.L., Musikhin Yu.G., Bert N.A., Kop'ev P.S., Alferov Zh.I., Ledentsov N.N., Bimberg D. *Appl. Phys. Lett.*, **74**, 2815 (1999).

34. Zhukov A.E., in *Landolt-Börnstein: Numerical Data and Functional Relationships in Science and Technology – New Series.* Ed. by H. Weber, P. Loosen, R. Poprawe (Berlin, Heidelberg, New York: Springer-Verlag, 2011) Vol. VIII/1B3, pp. 95–131.

35. Maximov M.V., Ustinov V.M., Zhukov A.E., Kryzhanovskaya N.V., Payusov A.S., Novikov I.I., Gordeev N.Yu., Shernyakov Yu.M., Krestnikov I., Livshits D., Mikhrin S., Kovsh A. *Semicond. Sci. Technol.*, **23**, 105004 (2008).

36. Amano T., Aoki S., Sugaya T., Komori K., Okada Y. *IEEE J. Sel. Top. Quantum Electron.*, **13**, 1273 (2007).

37. Freisem S., Ozgur G., Shavritranuruk K., Chen H., Deppe D.G. *Electron. Lett.*, **44**, 679 (2008).

38. Deppe D.G., Shavritranuruk K., Ozgur G., Chen H., Freisem S. *Electron. Lett.*, **45**, 54 (2009).

39. Tanaka Y., Ishida M., Maeda Y., Akiyama T., Yamamoto T., Song H.-Z., Yamaguchi M., Nakata Y., Nishi K., Sugawara M., Arakawa Y. *Conf. OFC* (San Diego, CA, USA, 2009) OWJ1.

40. Rayleigh L. *Philos. Mag.*, **20**, 1001 (1910).

41. Garrett C.G.B., Kaiser W., Bond W.L. *Phys. Rev.*, **124**, 1807 (1961).

42. Grudinin I.S., Ilchenko V.S., Maleki L. *Phys. Rev. A*, **74**, 063806 (2006).

43. Borselli M., Srinivasan K., Barclay P.E., Painter O. *Appl. Phys. Lett.*, **85**, 3693 (2004).

44. Borselli M., Johnson T.J., Painter O. *Opt. Express*, **13**, 1515 (2005).

45. Zhukov A.E., Maximov M.V., Gordeev N.Yu., Savelyev A.V., Kryzhanovskaya N.V., Shernyakov Y.M., Nadtochiy A.M., Payusov A.S., Zubov F.I., Korenev V.V. *Int. Conf. Nonlinear Optics/Laser, Applications and Technol. Conf.* (Moscow, Russia, 2013, Plenary 2).

46. Gorodetsky M.L. *Opticheskie mikrorezonatory s gigantskoi dobrotnost'yu* (Giant Q Optical Microresonators) (Moscow: Fizmatlit, 2011).

47. *Properties of Aluminum Gallium Arsenide.* Ed. by S. Adachi (London, UK: INSPEC, the Institution of Electrical Engineers, 1993).

48. Kryzhanovskaya N.V., Blokhin S.A., Maximov M.V., Nadtochy A.M., Zhukov A.E., Fedorova K.V., Ledentsov N.N., Ustinov V.M., Il'inskaya N.D., Bimberg D. *Fiz. Tekh. Poluprovodn.*, **45**, 992 (2011).

49. Astratov V.N., Yang S., Lam S., Jones B.D., Sanvitto D., Whittaker D.M., Fox A.M., Skolnick M.S., Tahraoui A., Fry P.W., Hopkinson M. *Appl. Phys. Lett.*, **91**, 071115 (2007).

50. Hill M.T., Anantathanasarn S., Zhu Y., Oei Y.-S., van Veldhoven P.J., Smit M.K., Nötzel R. *IEEE Photonics Technol. Lett.*, **20**, 446 (2008).

51. Mao M.-H., Chien H.-C., Hong J.-Z., Cheng C.-Y. *Opt. Express*, **19**, 14145 (2011).

52. Choquette K.D., Geib K.M., Ashby C.I.H., Twesten R.D., Blum O., Hou H.Q., Follstaedt D.M., Hammons B.E., Mathes D., Hull R. *IEEE J. Sel. Top. Quantum Electron.*, **3**, 916 (1997).

53. Srinivasan K., Borselli M., Johnson T.J., Barclay P.E., Painter O., Stintz A., Krishna S. *Appl. Phys. Lett.*, **86**, 151106 (2005).

54. Walther H., Varcoe B.T.H., Englert B.-G., Becker T. *Rep. Prog. Phys.*, **69**, 1325 (1996).

55. Ide T., Baba T., Tatebayashi J., Iwamoto S., Nakaoka T., Arakawa Y. *Appl. Phys. Lett.*, **85**, 1326 (2004).

56. Ide T., Baba T., Tatebayashi J., Iwamoto S., Nakaoka T., Arakawa Y. *Opt. Express*, **13**, 1615 (2005).

57. Yang T., Shchekin O., O'Brien J.D., Deppe D.G. *Electron. Lett.*, **39**, 1657 (2003).

58. Yang T., Cao J.-R., Lee P.-T., Shih M.-H., Shafiiha R., Farrell S.G., O'Brien J.D., Shchekin O., Deppe D.G. *Conf. CLEO* (Baltimore, ML, USA, 2003) CWK3.

59. Kryzhanovskaya N.V., Zhukov A.E., Nadtochy A.M., Slovinsky I.A., Maximov M.V., Kulagina M.M., Savelev A.V., Arakcheeva E.M., Zadiranov Yu.M., Troshkov S.I., Lipovskii A.A. *Fiz. Tekh. Poluprovodn.*, **46**, 1063 (2012).

60. McCaulley J.A., Donelly V.M., Veron M., Taha I. *Phys. Rev. B*, **49**, 7408 (1994).

61. Kryzhanovskaya N.V., Zhukov A.E., Nadtochy A.M., Maximov M.V., Moiseev E.I., Kulagina M.M., Savelev A.V., Arakcheeva E.M., Lipovskii A.A., Zubov F.I., Kapsalis A., Mesaritakis C., Syvridis D., Mintairov A., Livshits D. *Fiz. Tekh. Poluprovodn.*, **47**, 1396 (2013).

62. Kryzhanovskaya N.V., Blokhin S.A., Gladyshev A.G., Maleev N.A., Kuz'menkov A.G., Arakcheeva E.M., Tanklevskaya E.M., Zhukov A.E., Vasil'ev A.P., Semenova E.S., Maximov M.V., Ledentsov N.N., Ustinov V.M., Stock E., Bimberg D. *Fiz. Tekh. Poluprovodn.*, **40**, 1128 (2006).

63. Zhukov A.E., Kryzhanovskaya N.V., Savelyev A.V., Nadtochiy A.M., Arakcheeva E.M., Zubov F.I., Korenev V.V., Maximov M.V., Shernyakov Yu.M., Kulagina M.M., Slovinskiy I.A., Livshits D.A., Kapsalis A., Mesaritakis Ch., Syvridis D., Mintairov A. *Proc. SPIE Int. Soc. Opt. Eng.*, **8552**, 855202 (2012).

64. Nadtochy A.M., Kryzhanovskaya N.V., Maximov M.V., Zhukov A.E., Moiseev E.I., Kulagina M.M., Vashanova K.A., Zadiranov Yu.M., Mukhin I.S., Arakcheeva E.M., Livshits D., Lipovskii A.A. *Pis'ma Zh. Tekh. Fiz.*, **23**, 70 (2013).

65. Zhang L., Hu E. *Appl. Phys. Lett.*, **82**, 319 (2003).

66. Ushigome R., Fujita M., Sakai A., Baba T., Kokubun Y. *Jpn. J. Appl. Phys.*, **41**, 6364 (2002).

67. Munsch M., Claudon J., Malik N.S., Gilbert K., Grosse P., Gerard J.-M., Albert F., Langer F., Schlereth T., Pieczarka M.M., Hofling S., Kamp M., Forchel A., Reitzenstein S. *Appl. Phys. Lett.*, **100**, 031111 (2012).

68. Cao H., Deng H., Ling H., Liu C., Smagley V.A., Caldwell R.B., Smolyakov G.A., Gray A.L., Lester L.F., Eliseev P.G., Osiñski M. *Appl. Phys. Lett.*, **86**, 203117 (2005).

69. Van Campenhout J., Rojo-Romeo P., Regreny P., Seassal C., Van Thourhout D., Di Cioccio L., Lagahe C., Fedeli J.-M., Baets R. *Proc. SPIE Int. Soc. Opt. Eng.*, **6898**, 68980L (2008).

70. Liang D., Fiorentino M., Srinivasan S., Bowers J.E., Beausoleil R.G. *IEEE J. Sel. Top. Quantum Electron.*, **17**, 1528 (2011).

71. Marcatili E.A.J. *Bell Syst. Tech. J.*, **48**, 2103 (1969).

72. Varangis P.M., Li H., Liu G.T., Newell T.C., Stintz A., Fuchs B., Malloy K.J., Lester L.F. *Electron. Lett.*, **36**, 1544 (2000).

73. Kovsh A., Krestnikov I., Livshits D., Mikhrin S., Weimert J., Zhukov A. *Opt. Lett.*, **32**, 793 (2007).

74. Lee C.-S., Guo W., Basu D., Bhattacharya P. *Appl. Phys. Lett.*, **96**, 101107 (2010).

75. Rafailov E.U., Cataluna M.A., Sibbett W., Il'inskaya N.D., Zadiranov Yu.M., Zhukov A.E., Ustinov V.M., Livshits D.A., Kovsh A.R., Ledentsov N.N. *Appl. Phys. Lett.*, **87**, 081107 (2005).

76. Gubenko A., Krestnikov I., Livshits D., Mikhrin S., Kovsh A., West L., Bornholdt C., Grote N., Zhukov A. *Electron. Lett.*, **43**, 1430 (2007).

77. Xu Q., Schmidt B., Pradhan S., Lipson M. *Nature*, **435**, 325 (2005).

78. Soref R.A., Bennett B.R. *IEEE J. Quantum Electron.*, **23**, 123 (1987).

79. Van Campenhout J., Liu L., Romeo P.R., Van Thourhout D., Seassal C., Regreny P., Di Cioccio L., Fedeli J.-M., Baets R. *IEEE Photonics Technol. Lett.*, **20**, 1345 (2008).

80. Gubenko A., Kovsh A., Wojcik G., Livshits D., Krestnikov I., Mikhrin S. U.S. Patent 8, 411, 711 (2013).

81. Xu Q., Schmidt B., Shakya J., Lipson M. *Opt. Express*, **14**, 9430 (2006).

82. Dong P., Liao S., Feng D., Liang H., Zheng D., Shafiiha R., Kung C.-C., Qian W., Li G., Zheng X., Krishnamoorthy A.V., Asghari M. *Opt. Express*, **17**, 22484 (2009).

83. Xu Q., Manipatruni S., Schmidt B., Shakya J., Lipson M. *Opt. Express*, **15**, 430 (2007).

84. Manipatruni S., Qianfan X., Schmidt B., Shakya J., Lipson M. *IEEE Proc. Lasers and Electro-Optics Soc*. (Lake Buena Vista, FL, USA, 2007) p. 537.

85. Wojcik G.L., Yin D., Kovsh A.R., Gubenko A.E., Krestnikov I.L., Mikhrin S.S., Livshits D.A., Fattal D.A., Fiorentino M., Beausoleil R.G. *Proc. SPIE Int. Soc. Opt. Eng.*, **7230**, 72300M (2009).

86. Rasras M.S., Gill D.M., Patel S.S., White A.E., Tu K., Chen Y., Carothers D.N., Pomerene A.T., Grove M.J., Sparacin D., Michel J., Beals M.A., Kimerling L.C. *Conf. OFC* (Anaheim, CA, USA, 2006) PDP13.

87. Chen L., Sherwood-Droz N., Lipson M. *Opt. Lett.*, **32**, 3361 (2007).

88. Shen X., Han K., Liu H.-S., Li H., Tang G. *Int. Workshop Metamaterials* (Nanjing, China, 2008) p. 149.

89. Weiss D., Sandoghdar V., Hare J., Lef'evre-Seguin V., Raimond J., Haroche S. *Opt. Lett.*, **22**, 1835 (1995).

90. Little B.E., Laine J.T., Chu S.T. *Opt. Lett.*, **22**, 4 (1997).

91. Ikeda T., Hane K. *Appl. Phys. Lett.*, **102**, 221113 (2013).

92. Shamai R., Levy U. *Opt. Express*, **17**, 1116 (2009).